PHYSICAL REVIEW A **76**, 031403(R) (2007)

Fractal templates in the escape dynamics of trapped ultracold atoms

Kevin A. Mitchell
School of Natural Sciences, University of California, Merced, California 95344, USA

Daniel A. Steck
Oregon Center for Optics and Department of Physics, 1274 University of Oregon, Eugene, Oregon 97403-1274, USA

(Received 5 December 2006; published 17 September 2007)

We consider the dynamic escape of a small packet of ultracold atoms launched from within an optical dipole trap. Based on a theoretical analysis of the underlying nonlinear dynamics, we predict that fractal behavior can be seen in experimental escape data. These data can be collected by measuring the time-dependent escape rate for packets launched over a range of angles. This fractal pattern is particularly well resolved below the Bose-Einstein transition temperature—a direct result of the extreme phase-space localization of the condensate. We predict that several self-similar layers of this novel fractal should be measurable, and we explain how this fractal pattern can be predicted and analyzed with recently developed techniques in symbolic dynamics.

DOI: 10.1103/PhysRevA.76.031403 PACS number(s): 32.80.Pj, 05.45.Ac, 05.45.Df

Chaotic transport and escape underlie such diverse phenomena as conductance through ballistic microstructures [1], emission from deformed microdisk semiconductor lasers [2], molecular scattering and dissociation [3], celestial transport [4], and atomic ionization [5–7]. Although the phase space for such systems is well known to exhibit fractal features, these features typically influence experimental data via such quantities as fractal dimensions, asymptotic decay rates, and Lyapunov exponents. This paper proposes that ultracold atoms could be a valuable experimental tool to observe fine-scale self-similar fractal features directly.

We have been particularly motivated by the chaotic ionization of hydrogen in applied parallel electric and magnetic fields, for which a recent theoretical analysis [7] predicts that the time spectrum for ionization will display a *chaos-induced train* of electron pulses. This prediction is based on classical ionizing trajectories [Fig. 1(a)], which propagate from the nucleus into the ionization channel, via the Stark saddle. These trajectories exhibit fractal self-similarity, which is indirectly reflected in the pulse train. Although these predictions have been recently confirmed by full quantum calculations [8], their experimental observation remains unrealized.

In this paper, we consider an alternative chaotic system—the escape of ultracold atoms in specially tailored optical dipole traps. We propose that the flexibility and control afforded by cold atoms, especially in engineering the initial state, permit the *direct* imaging of fractals in the escape dynamics. Furthermore, we show how the fine-scale fractal self-similarity can be understood using a recently developed symbolic formalism. The fractals studied here result from homoclinic tangles [10]—a general mechanism for phase-space transport. Hence this paper suggests that cold atoms could serve as a unique high-precision experimental probe of this fundamental mechanism. Finally, the cold atom experiments discussed here are readily feasible with present-day experimental configurations and could prove easier to realize than the previously mentioned ionization experiments.

Recent experiments from the Raizen [11] and Davidson [12] groups have made first steps along these lines. They independently measured the *long-time* survival probability for ultracold atoms escaping through a hole in an optical billiard, demonstrating the distinction between regular and chaotic escape dynamics. In contrast, our work focuses on the short- to intermediate-time dynamics, where fundamentally distinct phenomena, such as fractal self-similarity, are predicted to appear.

Double-Gaussian trap. We consider a dipole potential consisting of two overlapping Gaussian wells,

$$V(x,y) = -V_1 \exp\{-[(x/\sigma_{1x})^2 + (y/\sigma_{1y})^2]/2\} - V_2 \exp(-\{[(x-x_2)/\sigma_{2x}]^2 + (y/\sigma_{2y})^2\}/2), \quad (1)$$

as shown in Fig. 1(b). This potential can be created by two red-detuned, far-off-resonant Gaussian beams; atomic motion can be further restricted transverse to the xy plane by a uniform laser sheet. Here, we take $\sigma_{1x}=0.18$, $\sigma_{1y}=0.24$, $\sigma_{2x}=1.08$, $\sigma_{2y}=0.24$, $x_2=0.72$ (measured in millimeters), and $V_1=V_2=35.5$ (measured in recoil energies $E_r=\hbar^2k_L^2/2m_{Rb}=h\times 3.77$ kHz, where $\lambda=2\pi/k_L=780.2$ nm for the D_2 transition of ^{87}Rb.) The double-Gaussian potential shares several features in common with the hydrogen potential in Fig. 1(a). The "primary" Gaussian centered at the origin is analogous to the Coulomb well, the elongated "secondary" Gaussian on the right is analogous to the ionization channel, and the saddle connecting the two Gaussian wells is analogous to the Stark saddle. We are interested in the transport of atoms from the primary well into the secondary well. Figure 1(b) shows two representative trajectories that move away from the ori-

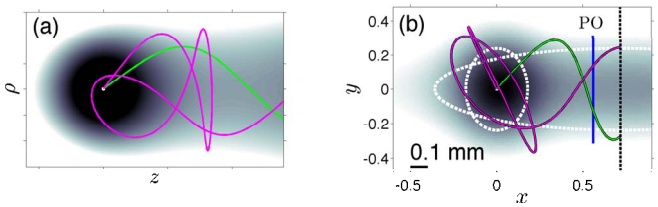

FIG. 1. (Color online) (a) The potential energy for a hydrogenic electron in applied parallel electric and magnetic fields. Two ionizing trajectories are shown. (b) The double-Gaussian potential. Gaussian widths are indicated by the dashed ellipses.

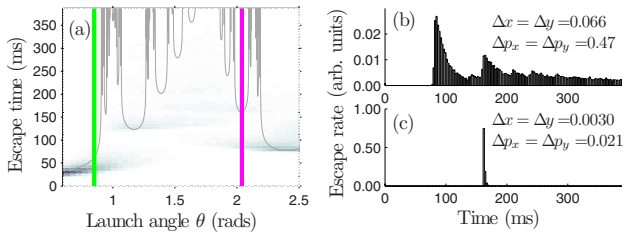

FIG. 2. (Color online) (a) Escape-time plot. The two vertical lines mark the launch angles for the trajectories in Fig. 1(b). Parts (b) and (c) show the flux of atoms at the detection line for two Gaussian ensembles launched at θ=2.04. The sharp pulse in (c) indicates that the Gaussian packet remains a well-localized packet throughout its trajectory, whereas the "train" of pulses in (b) indicates substantial breakup and mixing. The position and momentum widths of the initial ensembles are given in units of mm and recoil momenta ($p_r=\hbar k_L=m_{Rb}\times 5.88$ mm/s for the ^{87}Rb D_2 transition).

gin with initial speed 4.12 cm/s, pass over an unstable periodic orbit (PO) near the saddle, and then strike a resonant laser sheet (the vertical dashed line.) This sheet forms a *detection line*—upon striking the line, an atom scatters many resonant photons, providing a detectable measure of escape time as well as pushing the atom out of the trap, preventing its return into the primary well.

The sharp curves in Fig. 2(a) show the time for a trajectory with initial speed 4.12 cm/s (energy $-14.9E_r$) to move from the origin to the detection line, as a function of launch angle θ, measured in radians relative to the positive x axis. The resulting *escape-time plot* is highly singular, with numerous "icicles" whose edges tend toward infinity. These icicles exhibit a self-similar fractal pattern, common in chaotic escape and scattering [9].

A proposed experiment to measure self-similar patterns in the escape-time plot. We consider a small Gaussian packet of ultracold atoms launched from the origin with speed 4.12 cm/s and θ=2.04 [the right line in Fig. 2(a)]. The subsequent flux of atomic trajectories at the detection line is then computed as a function of time. Figure 2(b) shows this flux for an initial thermal packet that occupies a phase space area 500 times Planck's constant in both the x and y degrees of freedom (which corresponds here to a temperature T =75 nK). Figure 2(c), on the other hand, uses a packet that occupies a single Planck cell, appropriate for a pure dilute Bose-Einstein condensate (BEC) in the regime of negligible atom-atom interactions and $T\approx 0$ [13]. The condensate packet closely follows the trajectory in Fig. 1(b), exiting as a sharp pulse at 160 ms, near the bottom of the θ=2.04 icicle in Fig. 2(a). The thermal packet also produces a pulse at 160 ms, but its larger phase-space extent populates neighboring icicles, thereby producing the additional pulses in Fig. 2(b). For example, the large initial pulse is due to trajectories associated with the rightmost icicle in Fig. 2(a).

By repeating the preceding computation for different launch angles of the thermal packet, we obtain the aggregate data in Fig. 2(a), where the shading records the atomic flux as a function of arrival time and the packet's launch angle. Figure 2(b) then corresponds to the vertical slice through Fig. 2(a) at θ=2.04. The thermal data appear as a blurred

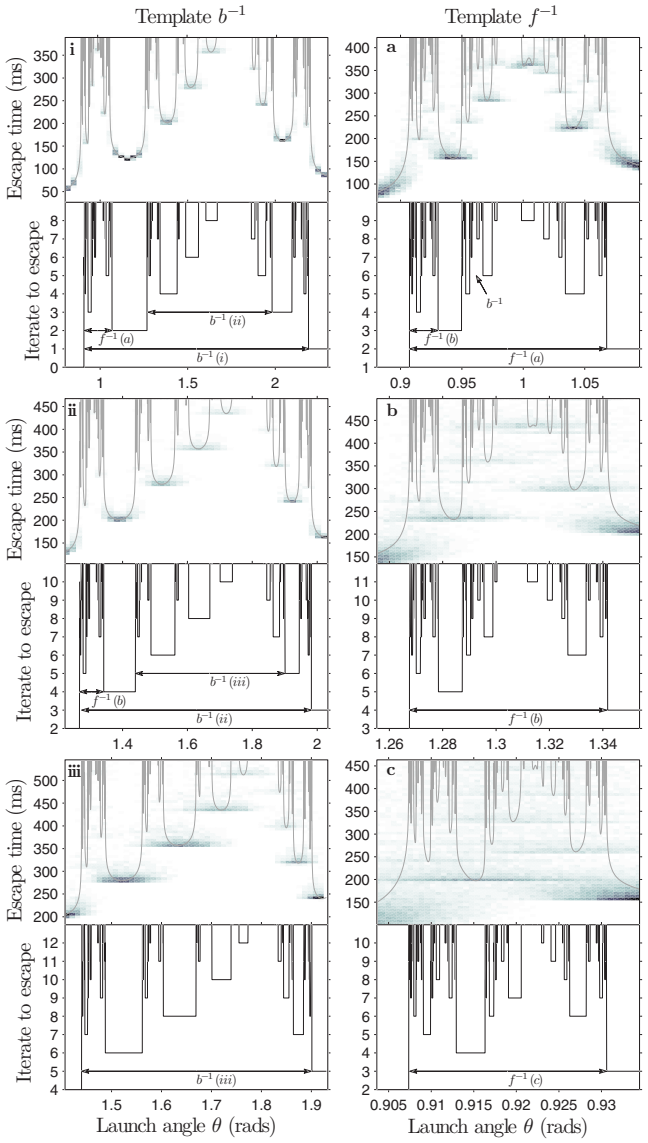

FIG. 3. (Color online) Escape time for a minimum uncertainty packet (BEC) over six angular intervals. The initial speed (4.12 cm/s) and widths Δx, Δy, Δp_x, and Δp_y are as in Fig. 2(c). (To check dependence on the initial width, we doubled the width and found a noticeable, but relatively small, impact on the fractal resolution.) Each escape-time plot is matched below by its corresponding discrete-escape-time plot.

version of the sharp escape-time plot. For example, the left and right icicles are associated with prominent dark patches and in between a few wispy patches can be associated with the bottoms of other icicles. Overall, however, the intricate icicle structure is poorly resolved by the thermal data.

A remarkable increase in resolution occurs below the BEC transition at $T\approx 0$, shown in Fig. 3(i). Many icicles are now clearly resolved, a direct consequence of the high phase-space localization afforded by the condensate.

Self-similarity of the escape-time data. The first column of Fig. 3 shows three distinct intervals of θ. The upper plots in each pair look remarkably similar, and icicles in one plot can be identified with icicles in the other two. In fact, this pattern of icicles occurs on all scales throughout the escape-time

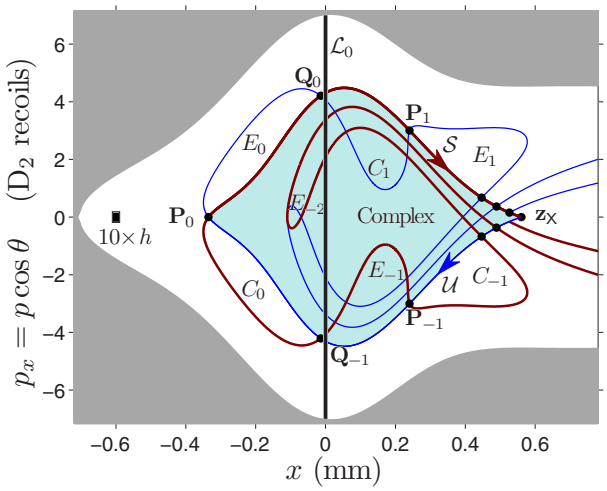

FIG. 4. (Color online) Surface of section with homoclinic tangle. The left rectangle has area 10 times Planck's constant.

plot. One of our principal observations is that these structures are resolved by the overlaid BEC data. The icicles look progressively more blurred as we move down the column because the interval width is decreasing and the escape time (and corresponding dispersion) is increasing.

The second column of Fig. 3 shows another pattern that also occurs on all scales throughout the *same* escape-time plot. As we will see, many such repeated patterns, or *templates*, exist in the escape-time plot. Within a given template, all other templates can be found on smaller scales in an infinitely recursive nesting. Our computations predict that several nested layers will be experimentally visible.

Experimentally, the observation of these phenomena will not be easy but certainly feasible. With a 1.06 μm laser, the above trap geometry can be realized with about 80 W of power. With this detuning, a ^{87}Rb atom has at most a 4% probability of spontaneous scattering over a half second. Acceleration of the atoms to the initial velocity of 4.12 cm/s is easily accomplished; for example, a chirped, one-dimensional optical lattice of 785 nm light with 50 mW of single-beam power and beam radius $w_0=100$ μm can accelerate the atoms in about 1.6 ms with negligible ($<1\%$) probability of spontaneous scattering and heating due to energy-band transitions. The primary difficulty is the subrecoil initial conditions required, even in the thermal case. However, a standard expanded BEC should suffice.

Theoretical foundations of the fractal structure. The self-similar fractal data can be described with recently developed symbolic tools [14]. We first specify a two-dimensional surface of section in the xyp_xp_y-phase space by fixing the energy E at $-14.9E_r$ and setting $y=0$. Thus, every time a trajectory passes through the x axis, we can record (x,p_x), defining a Poincaré map on the surface of section (Fig. 4). The vertical line $\mathcal{L}_0$ at $x=0$ consists of all points at the origin moving outward with arbitrary θ. The point $\mathbf{z}_X$ is the unstable fixed point equal to the intersection of the unstable periodic orbit in Fig. 1(b) with the surface of section. Attached to $\mathbf{z}_X$ are its stable $\mathcal{S}$ (thick) and unstable $\mathcal{U}$ (thin) manifolds, consisting of all points that converge to $\mathbf{z}_X$ in the forward and backward directions, respectively. These manifolds intersect an infinite number of times, forming an intricate pattern called a *homoclinic tangle* [10,14–16]. The stable and unstable segments connecting $\mathbf{z}_X$ to the point $\mathbf{P}_0$ bound the shaded region called the "complex."

Escape from the complex occurs via *escape lobes* E_n, defined as the regions bounded by the stable and unstable segments connecting $\mathbf{P}_n$ to $\mathbf{Q}_n$. The lobe E_{-1}, inside the complex, maps to E_0, outside the complex. Once in E_0, a point then maps to E_1, E_2, etc., eventually passing into the right well. The lobes E_{-k} contain all points that escape in k iterates. These lobes become progressively more stretched and folded as k increases. (The analogous lobes C_n control *capture* into the complex.) Note that we can choose physical parameters that make the lobes large compared to Planck's constant h (Fig. 4).

The lower plot of each pair in Fig. 3 shows the number of iterates to escape the complex as a function of θ. Each icicle is straightened into a constant escape segment. A segment that escapes on iterate k is an intersection between E_{-k} and $\mathcal{L}_0$. For example, the segment at iterate two in Fig. 3(i) is the intersection with E_{-2} in Fig. 4.

Reference [14] introduces a symbolic technique, called *homotopic lobe dynamics*, to compute the structure of escape segments based on the tangle topology. (See also Ref. [15].) We summarize the results obtained from applying this technique to the tangle in Fig. 4.

The structure of the discrete-escape-time plot up to a given iterate n is specified by a string ℓ_n of symbols in the set $\{c_1,c_2,a,b,f,u_0,u_1,u_2,\ldots\}$ as well as their inverses—e.g., c_1^{-1}. The first string is $\ell_1=u_1b^{-1}u_0$. All subsequent strings can be obtained from the first by mapping each symbol forward according to the substitution rules

$$c_1 \mapsto c_2, \quad c_2 \mapsto f^{-1}u_0au_0^{-1}f, \tag{2a}$$

$$a \mapsto b^{-1}u_0^{-1}b, \quad f \mapsto c_1^{-1}u_0^{-1}f, \tag{2b}$$

$$u_n \mapsto u_{n+1}, \quad b \mapsto b^{-1}u_0^{-1}f, \tag{2c}$$

using the standard convention for iterating inverses—e.g., $b^{-1}\mapsto f^{-1}u_0b$. For example, the first four strings are

$$\ell_1 = u_1b^{-1}\underline{u_0}, \tag{3a}$$

$$\ell_2 = u_2f^{-1}\underline{u_0}bu_1, \tag{3b}$$

$$\ell_3 = u_3f^{-1}\underline{u_0}c_1u_1b^{-1}\underline{u_0^{-1}}fu_2, \tag{3c}$$

$$\ell_4 = u_4f^{-1}\underline{u_0}c_1u_1c_2u_2f^{-1}\underline{u_0}bu_1^{-1}c_1^{-1}\underline{u_0^{-1}}fu_3. \tag{3d}$$

An ℓ_n string encodes the discrete-escape-time plot as follows. Each appearance of $u_0^{\pm1}$ in ℓ_n (underlined for emphasis) represents a segment that escapes at iterate n. For example, the u_0 factor in Eq. (3a) corresponds to the escape segment at iterate one in Fig. 3(i). This u_0 factor then maps forward to u_1 in Eq. (3b). In general, we see that each $u_k^{\pm1}$ in ℓ_n represents a segment that escapes at iterate $n-k$. In Eq. (3b), another u_0 factor has appeared, corresponding to the escape segment at iterate two. This segment is to the left of the first segment, just as the u_0 factor in Eq. (3b) is to the left of the

u_1 factor. In general, the left-right ordering of $u_k^{\pm 1}$symbols in ℓ_n represents the left-right ordering of segments in the discrete-escape-time plot. On the next two iterates, two new u_0 factors appear in Eq. (3c) and three more appear in Eq. (3d), in agreement with Fig. 3(i).

All other symbols besides $u_k^{\pm 1}$ represent gaps between adjacent escape segments. For example, b^{-1} in Eq. (3a) represents the gap $b^{-1}(i)$ in Fig. 3, and b^{-1} in Eq. (3c) represents the gap $b^{-1}(ii)$ in Figs. 3(i) and 3(ii). The string ℓ_5 will also contain a b^{-1} factor, representing the gap $b^{-1}(iii)$ in Figs. 3(ii) and 3(iii). Since each b^{-1} factor generates exactly the same string of symbols under Eqs. (2), each gap labeled b^{-1} in Fig. 3 contains the same pattern of escape segments. This means that b^{-1} corresponds to a particular template. Each symbol $\{c_1,c_2,a,b,f\}$ thus generates its own template, with inverse symbols generating reflected templates. For example, mapping f^{-1} forward 3 times yields $f^{-1}u_0c_1u_1c_2u_2f^{-1}u_0au_0^{-1}f$. The reader may verify that this equation describes the segments up to iterates 5, 7, and 6 in Figs. 3(a)–3(c). Note that different experimental parameters will yield different algebraic rules and different templates.

This algebraic formalism computes a minimal set of escape segments, but generally not all segments. That is, at later times, we typically find additional segments in the numerics. This illustrates what has previously been called an *epistrophic fractal* [16]. Nevertheless, unpredicted segments can be accommodated within an updated algebraic formalism, as explained in Ref. [14].

Conclusions. We predict that experiments on the intermediate-time escape dynamics of ultracold atoms from an optical trap can directly image self-similar fractals. The resolution is particularly good when using a minimum uncertainty packet (BEC). The fractal structure depends on the topology of homoclinic tangles, which are common to numerous chaotic systems. Such experiments would thus provide a new laboratory tool for the study of an important chaotic mechanism. Similarly, an improved understanding of the chaotic escape pathways of atoms from optical traps could be relevant for the understanding of mixing and thermalization in traps and for the control and coherent emission of atomic wave packets. Finally, the dependence of these fractals on atom density could serve as an interesting probe of atom-atom interactions, a subject to be explored in future work.

[1] R. Taylor *et al.*, *Electron Transport in Quantum Dots*, J. P. Bird ed. (Kluwer, Dordrecht, 2003).
[2] C. Gmachl *et al.*, Science **280**, 1556 (1998).
[3] M. J. Davis and S. K. Gray, J. Chem. Phys. **84**, 5389 (1986); M. J. Davis and R. E. Wyatt, Chem. Phys. Lett. **86**, 235 (1982); A. Tiyapan and C. Jaffé, J. Chem. Phys. **99**, 2765 (1993); **101**, 10393 (1994); **103**, 5499 (1995); F. Gabern *et al.*, Physica D **211**, 391 (2005); T. Uzer *et al.*, Nonlinearity **15**, 957 (2002).
[4] W. S. Koon *et al.*, Chaos **10**, 427 (2000); C. Jaffé *et al.*, Phys. Rev. Lett. **89**, 011101 (2002).
[5] R. V. Jensen, S. M. Susskind, and M. M. Sanders, Phys. Rep. **201**, 1 (1991); P. M. Koch and K. A. H. van Leeuwen, *ibid.* **255**, 289 (1995).
[6] R. Blümel and W. P. Reinhardt, *Chaos in Atomic Physics* (Cambridge University Press, Cambridge, England, 1997).
[7] K. A. Mitchell, J. P. Handley, B. Tighe, A. Flower, and J. B. Delos, Phys. Rev. Lett. **92**, 073001 (2004); Phys. Rev. A **70**, 043407 (2004).
[8] T. Topcu and F. Robicheaux, J. Phys. B **40**, 1925 (2007).
[9] For example, P. Gaspard, *Chaos, Scattering and Statistical Mechanics* (Cambridge University Press, Cambridge, England, 1998), and references therein.
[10] S. Wiggins, *Chaotic Transport in Dynamical Systems* (Springer-Verlag, New York, 1992).
[11] V. Milner, J. L. Hanssen, W. C. Campbell, and M. G. Raizen, Phys. Rev. Lett. **86**, 1514 (2001).
[12] N. Friedman, A. Kaplan, D. Carasso, and N. Davidson, Phys. Rev. Lett. **86**, 1518 (2001).
[13] The evolution of a localized quantum wave packet is well approximated by the evolution of a corresponding classical ensemble—e.g., S. Habib, e-print arXiv:quant-ph/0406011.
[14] K. A. Mitchell and J. B. Delos, Physica D **221**, 170 (2006).
[15] R. W. Easton, Trans. Am. Math. Soc. **294**, 719 (1986); V. Rom-Kedar, Physica D **43**, 229 (1990); Nonlinearity **7**, 441 (1994); B. Rückerl and C. Jung, J. Phys. A **27**, 6741 (1994); C. Lipp and C. Jung, *ibid.* **28**, 6887 (1995); C. Jung and A. Emmanouilidou, Chaos **15**, 023101 (2005); P. Collins, Int. J. Bifurcation Chaos Appl. Sci. Eng. **12**, 605 (2002); Dyn. Syst. **19**, 1 (2004); Dyn. Syst. **20**, 369 (2005); P. Collins, Exp. Math. **14**, 75 (2005).
[16] K. A. Mitchell *et al.*, Chaos **13**, 880 (2003); K. A. Mitchell *et al.*, *ibid.* **13**, 892 (2003).